Chapter 14
Operational Modal Analysis of a Rotating Structure Using a Novel Image-Based Long-Range Continuously Scanning Laser Doppler Vibrometer

L. F. Lyu and W. D. Zhu

Abstract A novel image-based long-range continuously scanning laser Doppler vibrometer (CSLDV) is developed to measure vibration of a rotating structure with a complex background. The image-based long-range tracking CSLDV can track and scan the rotating structure by processing its images captured by a camera in the image-based long-range tracking CSLDV. A novel image processing method with a background averaging technique is developed to extract the rotating structure from the background in captured images and determine its location. A one-dimensional scan scheme is used to scan along a straight line along the rotating structure. An improved demodulation method is used to process measurements of the image-based long-range tracking CSLDV to estimate modal parameters of the rotating structure, including damped natural frequencies and undamped mode shapes. Experiments of tracking and scanning a rotating blade are conducted to validate vibration measurements of a rotating blade using the image-based long-range tracking CSLDV. Measured responses of the rotating blade are processed to estimate its speeds and modal parameters. The first three one-dimensional damped natural frequencies of the rotating blade and undamped mode shapes along its middle line are successfully estimated and compared with results from the finite element model of the corresponding stationary blade.

Keywords Long-range laser Doppler vibrometer · Continuously scanning laser Doppler vibrometer · Image processing · Rotation tracking · Operational modal analysis

Introduction

A laser Doppler vibrometer (LDV) can measure the velocity of a point on a structure from the Doppler shift of the reflected laser beam of the LDV, which is an efficient way for noncontact vibration measurement of the structure [1]. A single-point LDV can only measure the vibration at one point on the structure each time, and it has to be moved to a new position to measure the vibration at another point. A scanning laser Doppler vibrometer (SLDV) was developed to increase the efficiency of vibration measurement [1–3]. A scanner with a set of orthogonal mirrors is used to reflect the laser beam of a single-point LDV in the SLDV. Mirrors of the scanner can rotate so that the laser spot of the SLDV can be moved to different positions while the SLDV is stationary. The SLDV measures the vibration of a point for some time and moves its laser spot to another point, which can provide vibration measurements on a grid on a structure. Measured responses on the grid can be used to estimate natural frequencies, mode shapes, and operational deflection shapes (ODSs) of the structure. To increase the spatial resolution of vibration measurement of a SLDV, a continuously scanning laser Doppler vibrometer (CSLDV) was developed [4–7]. Mirrors of the scanner in the CSLDV can continuously rotate so that the laser spot of the CSLDV can be continuously swept on the surface of a structure. One-dimensional (1D) and two-dimensional (2D) scan schemes were developed for the CSLDV to scan along different trajectories [7,8]. The CSLDV can be used to obtain full-field mode shapes and ODSs of stationary structures [8–10]. To measure vibration of a rotating structure, an image-based tracking CSLDV was developed [11–15], where a camera is integrated into the CSLDV to capture images of the rotating structure and determine its location. The image-based tracking CSLDV can only track and scan a rotating structure with a short distance from the CSLDV and reflective tapes are required to increase signal-to-noise ratios of measured responses. Hence, it is difficult to use

L. F. Lyu · W. D. Zhu
Department of Mechanical Engineering, University of Maryland, Baltimore County, 1000 Hilltop Circle, Baltimore, MD 21250
email: linfenl1@umbc.edu; wzhu@umbc.edu

Janko Slavic et al. (eds.), *Computer Vision & Laser Vibrometry, Vol. 6*, Conference Proceedings of the Society for Experimental Mechanics Series, https://doi.org/10.13052/97887-438-0151-1_14

the image-based tracking CSLDV for a large outdoor rotating structure, such as a rotating wind turbine blade.

Different operational modal analysis methods were developed to process measurement of a CSLDV [16–21]. A demodulation method was developed to estimate ODSs of a structure under sinusoidal excitation [16,17]. Measured responses of the structure are multiplied by sinusoidal signals whose frequencies are excitation frequencies, and processed responses are filtered by a low-pass filter to obtain ODSs of the structure. The demodulation method was improved to process measured responses of a structure under random excitation [12]. Measured responses of the structure are filtered by a band-pass filter that only contains a selected natural frequency, and filtered responses are multiplied by sinusoidal signals whose frequencies are the selected natural frequency. Multiplied responses are filtered by a low-pass filter to obtain undamped mode shapes of the structure. A lifting method was developed to estimate modal parameters of a structure under random excitation, such as damped natural frequencies, undamped mode shapes, and modal damping ratios [20,21]. The lifting method reconstructs measured responses of a CSLDV to obtain multiple measured responses at virtual measurement points as if there were vibration sensors attached to these points, which requires a high scan frequency of the CSLDV to estimate modes of a structure with high natural frequencies [11].

In this work, a novel image-based long-range tracking CSLDV is developed for tracking and scanning a relatively distant rotating structure with a complex background, which has application to a rotating wind turbine blade. A new image processing method with a background averaging technique is developed to remove backgrounds in images of the rotating structure captured by the camera in the image-based long-range tracking CSLDV. A 1D scan scheme is used for sweeping the laser spot of the image-based long-range tracking CSLDV, and the improved demodulation method is used to process its measurements. A rotating blade that is excited by air flow from an excitation fan is set up as a rotating structure that is tracked and scanned by the image-based long-range tracking CSLDV. Damped natural frequencies and undamped modes shapes of the rotating blade with different speeds are estimated.

Methodologies

To extract a rotating structure from a complex background, a novel background averaging method is developed here. A rotating fan is used as an example of a rotating structure for describing the background averaging method. A captured image of the rotating fan with a complex background is shown in Figure 1(a). Let the total number of captured images be *N*, and p_i is the *i*-th captured image, where $i = 1, 2, 3, \ldots, N$; the averaged image is

$$p_a = \frac{1}{N}\sum_{i=1}^{N} p_i \tag{1}$$

which is shown in Figure 1(b), where the hub and background remain in the image while blades of the fan are averaged out and would disappear with a sufficiently large *N*. Note that pixel values in the averaged image p_a should be integers, and one may need to apply a rounding function to the right-hand side of Equation (1). To extract blades of the fan from the background, one needs to obtain the difference between p_i and p_a:

$$p_i^{'} = |p_i - p_a| \tag{2}$$

The result of $|p_i - p_a|$ in Equation (2) is shown in Figure 1(c), where locations of blades can be easily determined by a common edge detection method [22]. Note that the robust edge detection method in [15] can also determine the location of a rotating structure with a complex background; however, this method can only be applied to a rotating structure with a non-zero speed, while the averaged image p_a in the present work can be applied to a stationary structure. Once edges of blades are located, a distance condition is used to track the location of an edge point on one of the blades [14].

When the distance between an image-based tracking CSLDV and the rotating blade that is scanned is long enough, rotation angles of mirrors of the scanner in the image-based tracking CSLDV are small and the location of the laser spot on the blade is generally linearly related to rotation angles of mirrors of the scanner [11]. Pixel coordinates of the laser spot in captured images of the camera in the image-based tracking CSLDV are linearly related to the location of the laser spot on the rotating blade when the camera is close to the scanner; thus pixel coordinates of the laser spot at time instant t in captured images are generally linearly related to rotation angles of mirrors of the scanner at time instant t. Once the location of the rotating blade that needs to be tracked is determined in captured images, a 1D scan path can be generated on the blade and rotation angles of mirrors of the scanner can be controlled so that the laser spot of the image-based tracking CSLDV can be swept along the path. Let the location of the edge point in the processed image $p_i^{'}$ determined by the edge detection method and distance condition be $(x_e,\ y_e)$, where the x axis and y axis are along the horizontal and vertical directions of $p_i^{'}$,

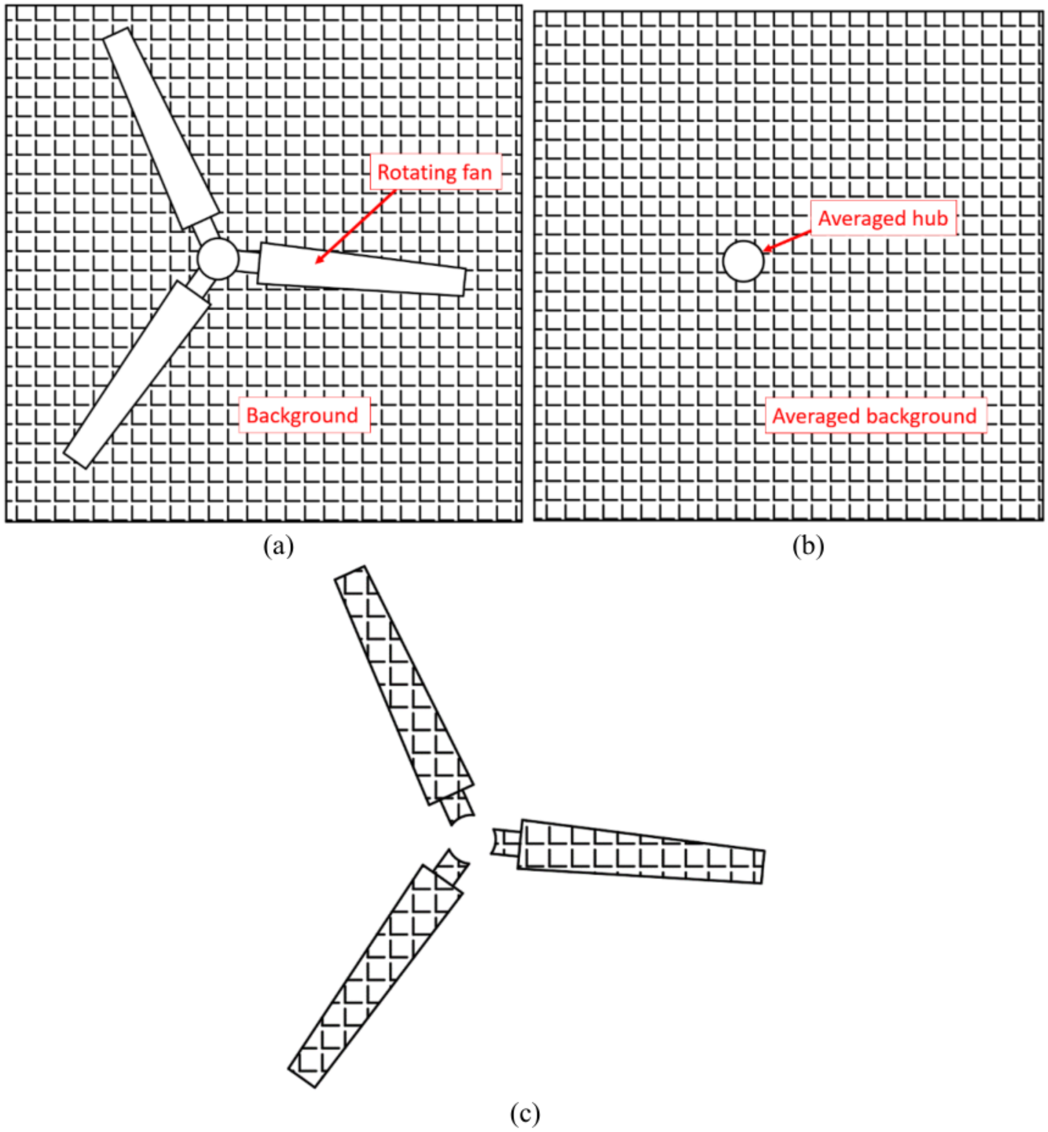

Fig. 1 (a) Schematic of a captured image of the rotating fan, (b) the averaged image of captured images of the rotating fan, and (c) the resulting image by subtracting the image in (b) from that in (a)

respectively, and the location of one end point of a straight scan path along the middle line of the rotating blade is

$$\begin{aligned} x_1 &= x_c + c[(x_e - x_c)\cos\theta + (y_e - y_c)\sin\theta] \\ y_1 &= y_c + c[(y_e - y_c)\cos\theta - (x_e - x_c)\sin\theta] \end{aligned} \tag{3}$$

where (x_c, y_c) is the location of the rotation center of the blade, c is a constant coefficient, and θ is the angle between the line passing through $(x_e,\ y_e)$ and (x_c, y_c) and the middle line of the blade. When locations of two end points of a straight scan path are determined, the laser spot can be swept along the straight path between them (Figure 2).

Once vibration measurement of the rotating blade is completed, measured responses of the rotating blade under random excitation can be processed by the improved demodulation method [12]. Fast Fourier transforms (FFTs) of measured responses are obtained to estimate damped natural frequencies of the rotating blade. Measured responses are filtered by a bandpass filter that only contains a selected damped natural frequency, and filtered responses are multiplied by sinusoidal signals whose frequencies are the selected damped natural frequency. A low-pass filter is applied to resulting responses to obtain the undamped mode shape associated with the selected damped natural frequency.

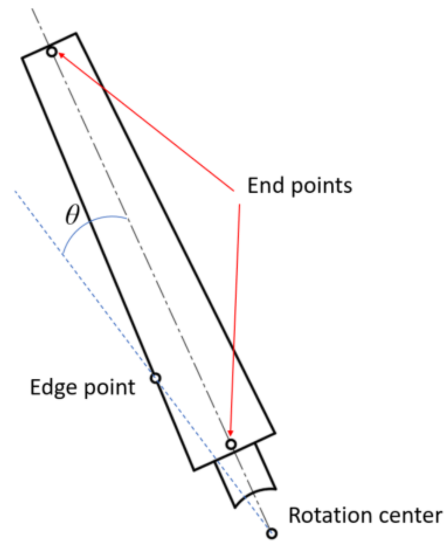

Fig. 2 Schematic of generating two end points of the straight scan path based on the location of the edge point.

Experiment and Results

The image-based long-range tracking CSLDV consists of a Polytec RSV-150 remote sensing vibrometer, a Cambridge 6240H scanner with a pair of orthogonal mirrors, a Basler acA1300-200um camera, and an NI controller (Figure 3(a)). An aluminum base was machined to hold the laser vibrometer, the camera, and the scanner (Figure 3(b)). The image-based long-range tracking CSLDV was placed in front of the rotating blade with a distance of 5.37 m (Figure 3(c)). Three aluminum blades were attached to a fan hub and one of them was scanned by the image-based long-range tracking CSLDV, and the fan hub was mounted on an aluminum frame (Figure 3(d)). A speed controller was connected to the hub so that it could rotate with different constant speeds. Lengths of middle lines, widths, and thicknesses of blades were 0.8 m, 0.1 m, and 3 mm, respectively. A finite element model of a stationary blade was used to estimate its undamped natural frequencies and undamped mode shapes via finite element method (FEM) simulations in ABAQUS (Figure 3(e)). The model was a clamped-free plate and shell elements were used in the model. The Young's modulus of the model was 70×10^9 Pa, the density was 2700 kg/m^3, and the Poisson's ratio was 0.35. A small fan was used to excite the rotating blades by its air flow, which could be considered as random excitation. The frame rate of the camera was set to 50 frames per second and the scan frequency of the scanner, which is the number of times the laser spot is swept back and forth along generated scan paths on the rotating blade in one second, was set to 0.625 Hz.

The position of the image-based long-range tracking CSLDV was adjusted so that the initial position of its laser spot was at the center of the hub. The hub was turned on and rotated with a constant speed, and the camera captured a sufficient number of images of the rotating blade. Captured images were used to obtain an averaged image, which was used as a background. Once the averaged image was obtained, it was used to remove backgrounds in images of the rotating blade when the image-based long-range tracking CSLDV scanned the blade.

Three of 1000 captured images of the three rotating blades are shown in Figures 4(a)-(c). The 1000 images were used to obtain an averaged image (Figure 4(d)). Three blades were eliminated in the averaged image while the hub was still in the image. The averaged image was subtracted from captured images to obtain images that only contain three blades (Figures 5(a)-(c)). The Sobel operator was applied to resulting images by subtracting the averaged image from captured images and their edge maps were obtained (Figures 5(d)-(f)) [22]. Note that there were some detected edges within boundaries of blades (Figures 5(d)-(f)), which did not affect tracking of one of the three blades since they did not appear outside boundaries of blades. There were detected edges at the location of the fan hub (Figures 5(d)-(f)), which was caused by the difference between the averaged hub image and the hub image at a certain instant during the hub's rotation.

A square region whose center was the hub center was used to extract a local region of interest (ROI) of the rotating blade that was tracked from an original captured image (Figure 6(a)). The pixel size of the ROI was 601×601 and the pixel location of the hub center in the ROI was (301, 301). Note that locations of boundary points of the ROI were determined by the pixel location of the hub center in the original image in Figure 6(a), and the pixel location of the hub center in the original image was determined by finding the center of the circular boundary of the hub (Figure 6(b)). Edges of rotating blades in

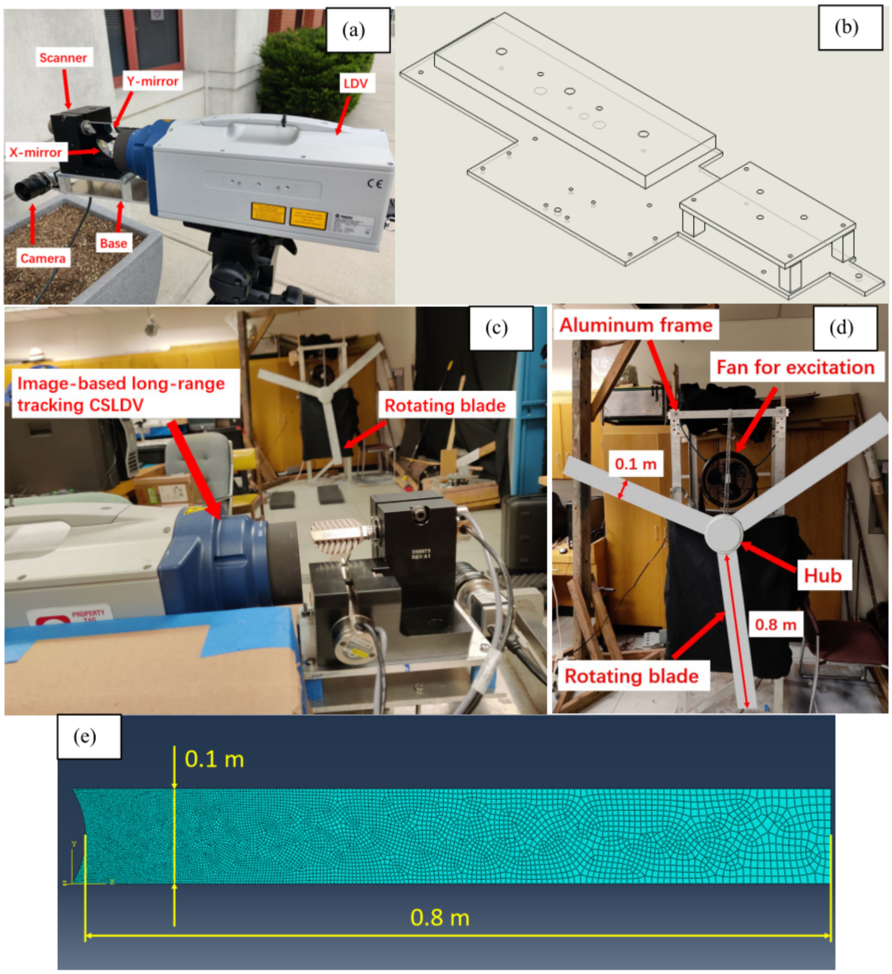

Fig. 3 (a) Picture of the image-based long-range tracking CSLDV, (b) the schematic of the aluminum base in (a), (c) the experimental setup for tracking and scanning a rotating blade using the image-based long-range tracking CSLDV, (d) the setup of the rotating blade, and (e) the finite element model of the rotating blade.

the ROI are shown in Figure 6(c), where an edge detection point whose position was (155, 551) in the ROI was used for the distance condition [14]. A set of inner and outer radial bounds whose centers are the hub center were used to determine edges within the two bounds, and radii of inner and outer radial bounds were 275 pixels and 300 pixels, respectively. Distances between the edge tracking point and edges within the two bounds were calculated and edges with distances smaller than a certain value (50 pixels in this work) were selected. The location of the geometric center of selected edges was calculated and used as an updated edge tracking point for the next captured image after the image shown in Figure 6(a). The updated edge tracking point was used as the edge position of the rotating blade that was tracked.

Estimated edge positions were used to generate scan paths on the rotating blade, and the laser spot of the image-based long-range tracking CSLDV was swept along them by rotating mirrors of the scanner. X- and Y-mirror signals of the scanner when scanning the rotating blade with different speeds, which were normalized by dividing them by their maximum values, are shown in Figure 7. X-mirror signals corresponded to horizontal movements of the laser spot and Y-mirror signals corresponded to vertical movements of the laser spot. Note that the stationary blade that was scanned was essentially at a vertical position so that the Y-mirror signal was much larger than the X-mirror signal.

Mirror signals were processed by calculating root sum squares of X- and Y-mirror signals [11]. Processed mirror signals were used for the improved demodulation method to determine end-to-end undamped mode shapes of the rotating blade [12]. Note that mirror signals when scanning the stationary blade were not processed since their shapes were the same as those obtained by calculating root sum squares of X- and Y-mirror signals. One can see that processed mirror signals with different rotation speeds were nearly the same since scan frequencies were the same when scanning the rotating blade with different rotation speeds (Figures 8(a) and (b)). Mirror signals in Figure 7 were also used to obtain rotation speeds of the

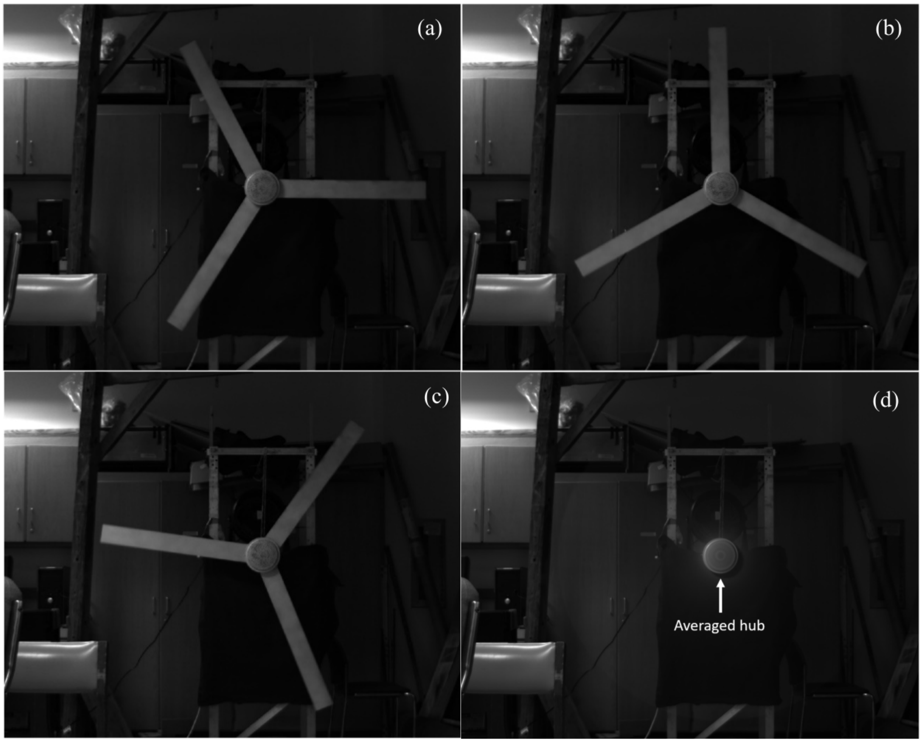

Fig. 4 (a) 50th, (b) 90th, and (c) 150th captured images of the camera, and (d) the averaged image.

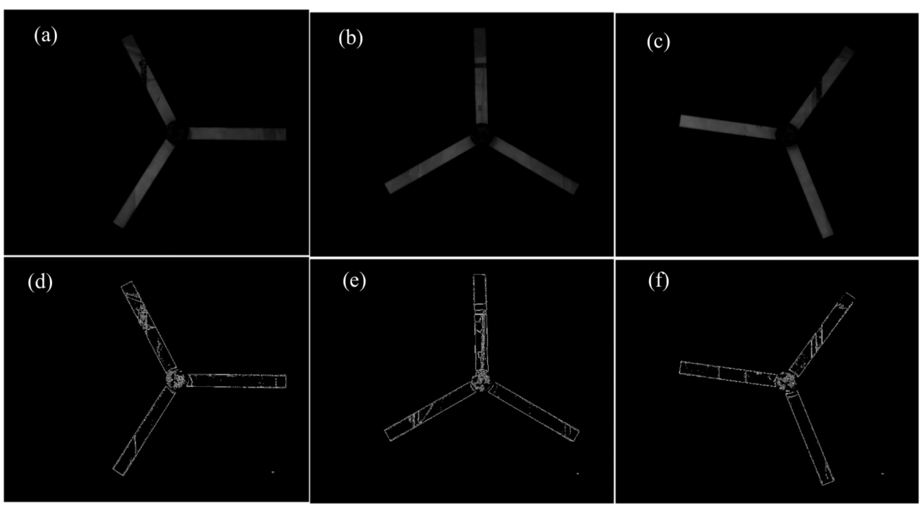

Fig. 5 Resulting images by subtracting the averaged image from (a) the 50th, (b) 90th, and (c) 150th captured images of the camera, and edge maps obtained from (d) the resulting image in (a), (e) the resulting image in (b), and (f) the resulting image in (c).

blade (Figure 8(c)). X- and Y- mirror signals were linearly related to horizontal and vertical positions of the laser spot, and they were converted to angular positions and velocities of the laser spot. Since the laser spot was swept along the blade, its angular velocities could be considered as rotation speeds of the blade. Estimated average rotation speeds of the blade with low and high speeds were 15.38 revolutions per minute (rpm) and 32.22 rpm, respectively.

Measured responses of the rotating blade with different speeds are shown in Figure 9. Note that there were outliers in measured responses that were caused by measurement noise of the long-range LDV, and they could be eliminated by some signal processing methods, such as an interpolation method. Damped natural frequencies of the rotating blade were estimated from FFTs of measured responses (Table 1). Note that damped natural frequencies of the stationary blade were somewhat

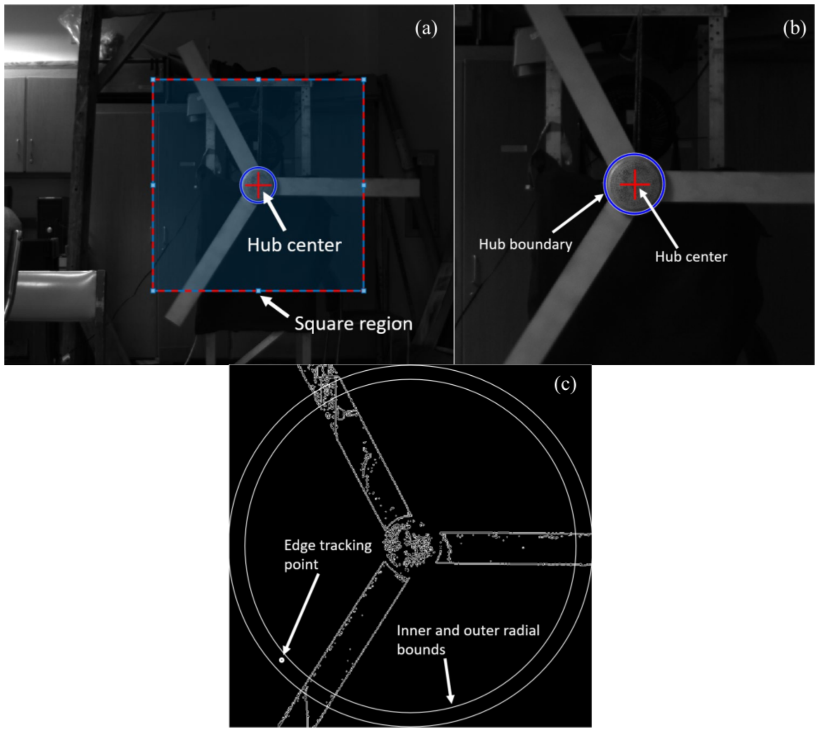

Fig. 6 (a) Original captured image with a square ROI, (b) the ROI, and (c) detected edges in the ROI.

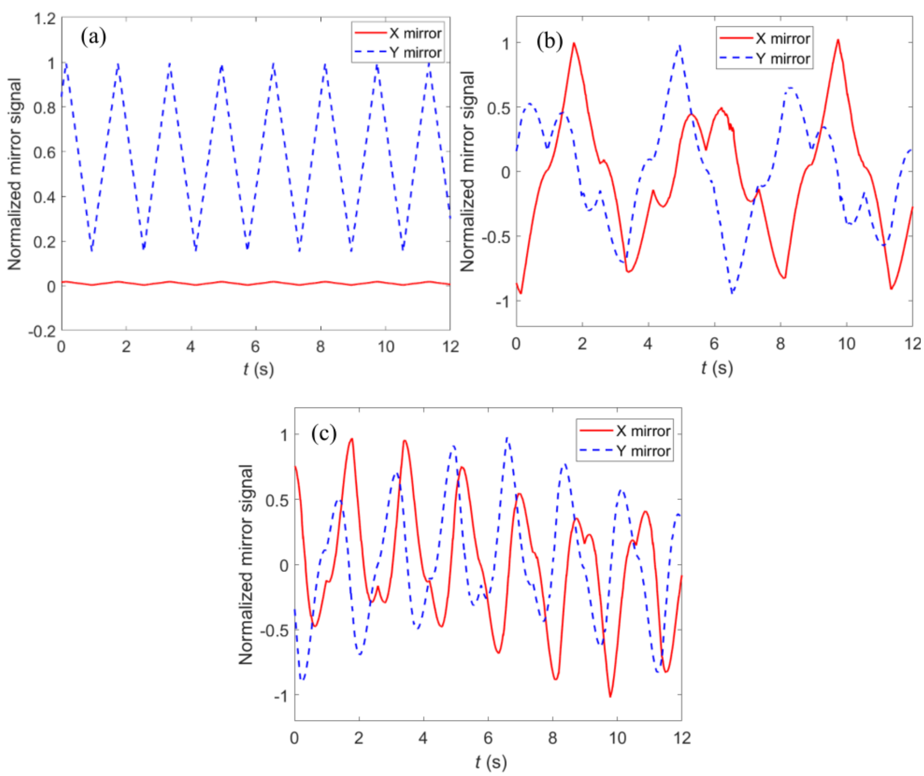

Fig. 7 Normalized mirror signals when scanning (a) the stationary blade, (b) the rotating blade with a low speed, and (c) the rotating blade with a high speed.

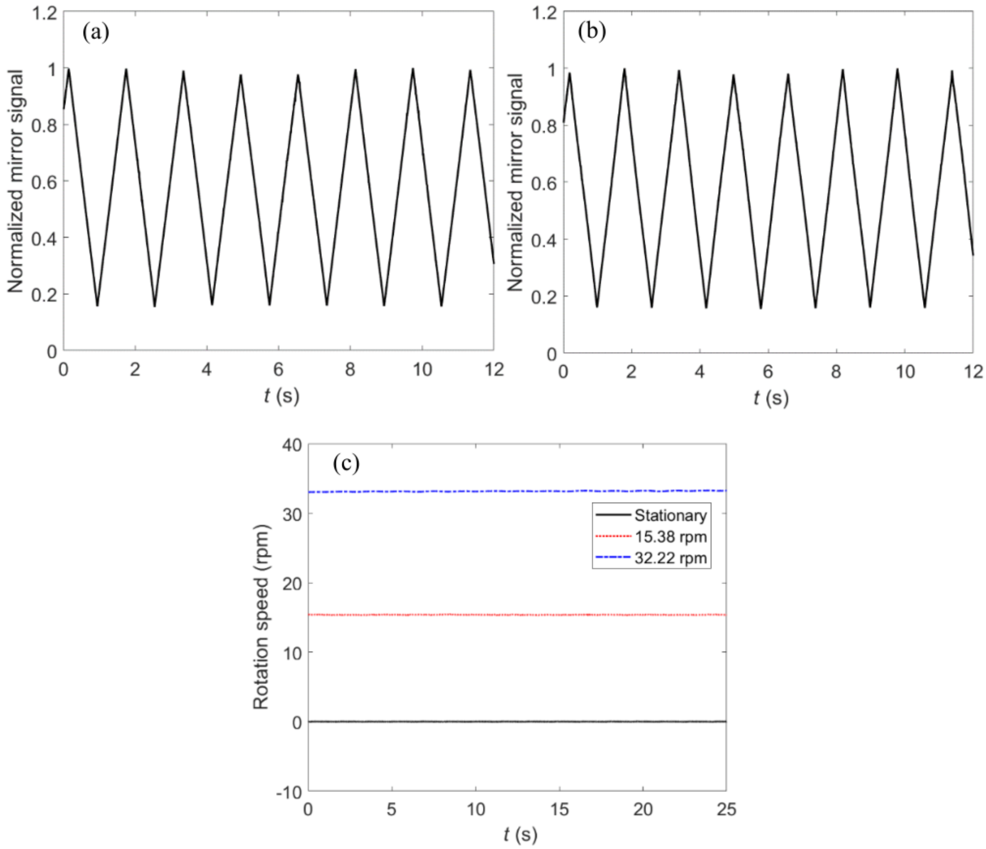

Fig. 8 Normalized processed mirror signals when scanning (a) the rotating blade with a low speed and (b) the rotating blade with a high speed, and (c) estimated rotation speeds of the blade.

Table 1 Estimated damped natural frequencies of stationary and rotating blades and undamped natural frequencies of the stationary blade from the finite element model.

	First damped natural frequency	Second damped natural frequency	Third damped natural frequency
FEM	1.63 Hz	10.19 Hz	28.55 Hz
Stationary	1.31 Hz	8.97 Hz	27.36 Hz
15.38 rpm	1.547 Hz	9.39 Hz	27.96 Hz
32.22 rpm	1.656 Hz	9.55 Hz	28.61 Hz

lower than those from FEM simulations (Table 2), which was due to the facts that the blade in the experiment was not perfectly clamped and there was some damping in the experiment while there was no damping in the finite element model. Estimated damped natural frequencies of the blade increased with its rotation speed, which was caused by the stiffening effect due to rotation [11–15].

Table 2 Differences between estimated damped natural frequencies of stationary and rotating blades and undamped natural frequencies of the stationary blade from the finite element model.

	First damped natural frequency	Second damped natural frequency	Third damped natural frequency
Stationary & FEM	19.63%	11.97%	4.17%
15.38 rpm & FEM	5.09%	7.85%	2.07%
32.22 rpm & FEM	-1.60%	6.28%	-0.21%

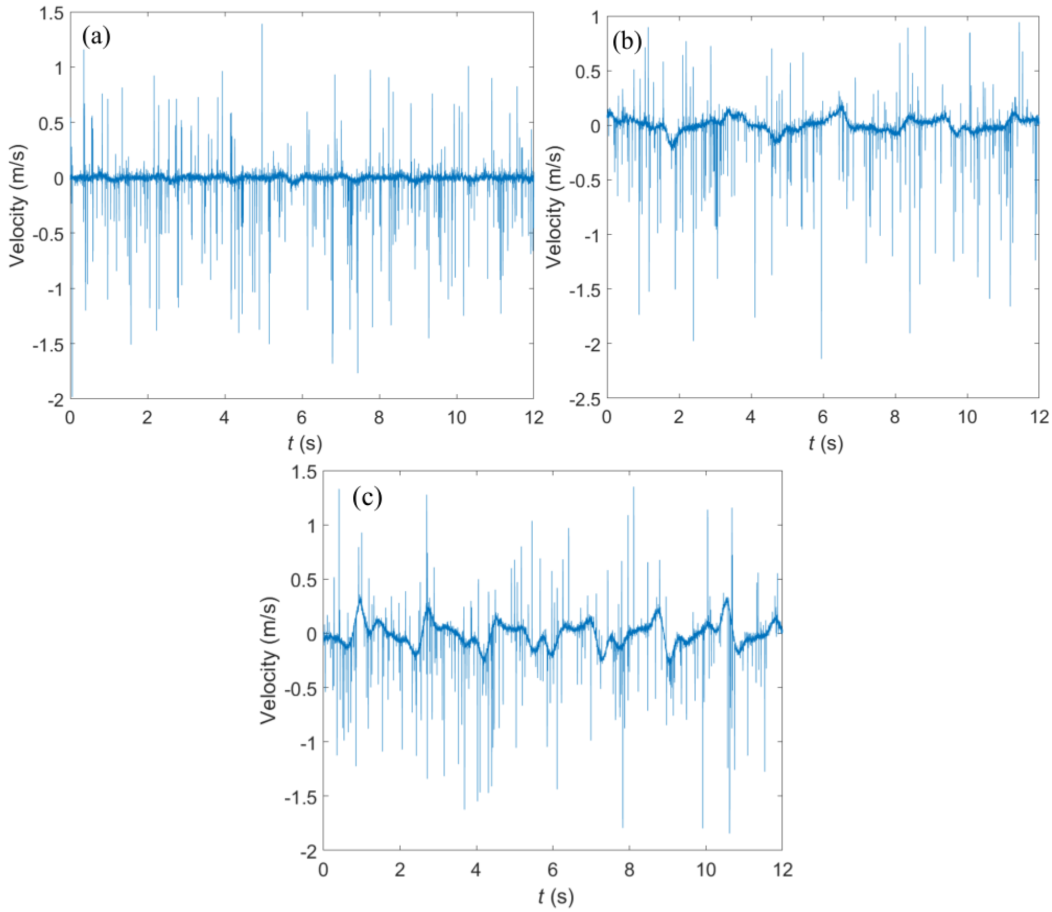

Fig. 9 Normalized processed mirror signals when scanning (a) the stationary blade, (b) the rotating blade with a speed of 15.38 rpm, and (c) the rotating blade with a speed of 32.22 rpm.

The improved demodulation method was applied to measured responses and processed mirror signals to estimate undamped mode shapes of the rotating blade. The estimated first three undamped bending mode shapes of the rotating blade with different speeds and first three undamped bending mode shapes of the stationary blade from the finite element model are shown in Figure 10. Estimated undamped mode shapes of the rotating blade are similar to bending mode shapes of a cantilever beam. Modal assurance criteria (MAC) values between estimated undamped mode shapes of the rotating blade and undamped mode shapes of the stationary blade from the finite element model were calculated (Table 3). MAC values are relatively high (over 95%) except for the value between the estimated third undamped mode shape of the rotating blade with a speed of 32.22 rpm and the undamped third mode shape of the stationary blade from the finite element model (93.85%), which could be caused by the stiffening effect due to rotation, differences in boundary conditions, and some inaccuracy of scanning the same path on the rotating blade with a high speed. Note that only 1D bending mode shapes of the rotating blade were estimated. To estimate torsional mode shapes of the rotating blade, a 2D scan scheme needs to be developed to scan its whole surface [15]. To estimate in-plane modes of the rotating blade, a 3D CSLDV system needs to be developed to measure 3D vibrations of the rotating blade [23–26].

Table 3 MAC values between estimated undamped mode shapes of stationary and rotating blades and undamped mode shapes of the stationary blade from its finite element model.

	First mode	Second mode	Third mode
Stationary & FEM	99.98%	99.83%	99.20%
15.38 rpm & FEM	99.93%	98.95%	96.64%
32.22 rpm & FEM	99.97%	98.37%	93.85%

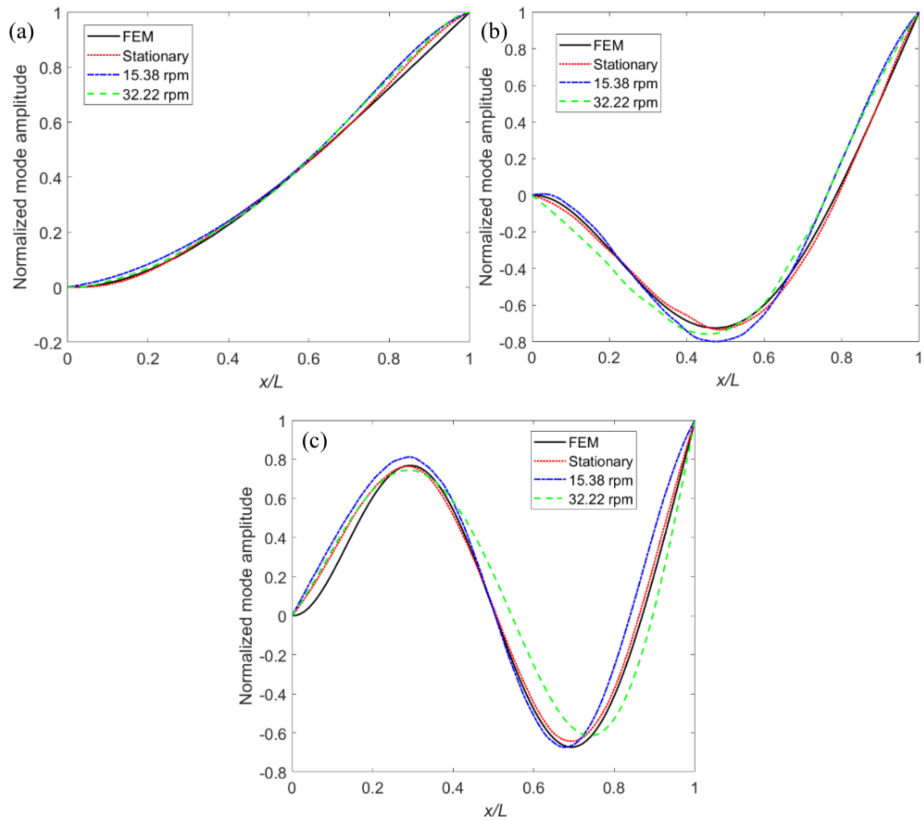

Fig. 10 Normalized estimated (a) first, (b) second, and (c) third undamped mode shapes when scanning the stationary blade, the rotating blade with a speed of 15.38 rpm, the rotating blade with a speed of 32.22 rpm, and the mode shape captured from the FEM results.

Conclusion

A novel image-based long-range tracking CSLDV was developed for tracking and scanning a rotating structure under random excitation with a long distance from the CSLDV. A novel image-processing method for tracking the rotating structure with a complex background was developed. The image-processing method includes a background averaging method and an edge detection method with a distance condition. The background averaging method can obtain the background of captured images of the rotating structure and remove it from captured images. The edge detection method can obtain the location of the rotating structure and track it. A 1D scan scheme was used to generate a straight scan path between its two end points on the structure based on its obtained location. An improved demodulation method was used to estimate damped natural frequencies and undamped mode shapes of the rotating structure. A rotating blade under air flow excitation was tracked and scanned by the image-based long-range tracking CSLDV, and its rotation speed, damped natural frequencies, and 1D undamped mode shapes were successfully estimated and compared with results from the finite element model of the corresponding stationary blade. The image-based long-range tracking CSLDV can be used to measure vibrations of outdoor rotating structures, such as rotating wind turbine blades.

Acknowledgments This research was supported by the National Science Foundation through Grant No. CMMI-1763024. The authors would like to thank Dan Feng for some valuable discussion on the background averaging method.

References

1. S. Rothberg, M. Allen, and P. Castellini, An international review of laser Doppler vibrometry: making light work of vibration measurement, Opt. Lasers Eng. 99(1) 11–22 (2017). https://doi.org/10.1016/j.optlaseng.2016.10.023.
2. B. Stoffregen, and A. Felske, Scanning laser Doppler vibration analysis system. *SAE Transactions*, 94(2) 934–940 (1985).

3. P. Castellini, M. Martarelli, and E. Tomasini, Laser Doppler vibrometry: development of advanced solutions answering to technology's needs. *Mech. Syst.* Signal Process. 20(6) 1265–1285 (2006). https://doi.org/10.1016/j.ymssp.2005.11.015.
4. P. Sriram, S. Hanagud, J. Craig, and N.M. Komerath, Scanning laser Doppler technique for velocity profile sensing on a moving surface, *Appl. Opt.* 29(16) 2409–2417 (1990). https://doi.org/10.1364/AO.29.002409.
5. P. Sriram, S. Hanagud, and J. Craig, Mode shape measurement using a scanning laser Doppler vibrometer, *Int. J. Anal. Exp. Modal Anal*. 7(3) 169–178 (1992).
6. M.S. Allen, and M.W. Sracic, A new method for processing impact excited continuous-scan laser Doppler vibrometer measurements, *Mech. Syst. Signal Process.* 24(3) 721–735 (2010). https://doi.org/10.1016/j.ymssp.2009.11.004.
7. D.M. Chen, Y.F. Xu, and W.D. Zhu, Damage identification of beams using a continuously scanning laser Doppler vibrometer system, *J. Vib. Acoust.* 138(5) 05011 (2016). https://doi.org/10.1115/1.4033639.
8. D.M. Chen, Y.F. Xu, and W.D. Zhu, Identification of damage in plates using full-field measurement with a continuously scanning laser Doppler vibrometer system, *J. Sound Vib.,* 422, 542–567 (2018). https://doi.org/10.1016/j.jsv.2018.01.005.
9. D.M. Chen, Y. F. Xu, and W.D. Zhu, Non-model-based identification of delamination in laminated composite plates using a continuously scanning laser Doppler vibrometer system, *J. Vib. Acoust.* 140(4) 041001 (2018). https://doi.org/10.1115/1.4038734.
10. D.M. Chen, Y.F. Xu, and W.D. Zhu, A comprehensive study on detection of hidden delamination damage in a composite plate using curvatures of operating deflection shapes, *J. Nondestruct. Eval.,* 38 54 (2019). https://doi.org/10.1007/s10921-019-0591-8.
11. L.F., Lyu, and W.D. Zhu, Operational modal analysis of a rotating structure under ambient excitation using a tracking continuously scanning laser Doppler vibrometer system, *Mech. Syst. Signal Process.* 152 107367 (2021). https://doi.org/10.1016/j.ymssp.2020.107367.
12. L.F., Lyu, and W.D. Zhu, Operational modal analysis of a rotating structure subject to random excitation using a tracking continuously scanning laser Doppler vibrometer via an improved demodulation method, *J. Vib. Acoust.* 144(1) 011006 (2021). https://doi.org/10.1115/1.4051178.
13. L.F. Lyu, and W.D. Zhu, Full-field mode shape estimation of a rotating structure subject to random excitation using a tracking continuously scanning laser Doppler vibrometer via a two-dimensional scan scheme, *Mech. Syst. Signal Process.* 169 108532 (2022). https://doi.org/10.1016/j.ymssp.2021.108532
14. L.F. Lyu, G.D. Higgins, and W.D. Zhu, Operational modal analysis of a rotating structure using image-based tracking continuously scanning laser Doppler vibrometry via a novel edge detection method, J. Sound Vib., 525 116797 (2022). https://doi.org/10.1016/j.jsv.2022.116797
15. L.F. Lyu, G.D. Higgins, and W.D. Zhu, A novel robust edge detection method for full-field modal parameter estimation using an image-based tracking continuously scanning laser Doppler vibrometer system. *Mech. Syst. Signal Process*., 195, 110242 (2023). https://doi.org/10.1016/j.ymssp.2023.110242.
16. A. Stanbridge, and D. Ewins, Modal testing using a scanning laser Doppler vibrometer, *Mech. Syst. Signal Process.* 13(2) 255–270 (1999). https://doi.org/10.1006/mssp.1998.1209.
17. D. Di Maio, and D. Ewins, Continuous scan, a method for performing modal testing using meaningful measurement parameters; Part I, *Mech. Syst. Signal Process.* 25(8) 3027–3042 (2011). https://doi.org/10.1016/j.ymssp.2011.05.018.
18. Y.F. Xu, D.M. Chen, and W.D. Zhu, Damage identification of beam structures using free response shapes obtained by use of a continuously scanning laser Doppler vibrometer system, *Mech. Syst. Signal Process.* 92 226–247 (2017). https://doi.org/10.1016/j.ymssp.2016.12.042.
19. Y.F. Xu, D.M. Chen, and W.D. Zhu, Modal parameter estimation using free response measured by a continuously scanning laser Doppler vibrometer system with application to structural damage identification, *J. Sound Vib.* 485 115536 (2020). https://doi.org/10.1016/j.jsv.2020.115536.
20. S. Yang, and M.S. Allen, Lifting approach to simplify output-only continuous-scan laser vibrometry, *Mech. Syst. Signal Process.* 45(2) 267–282 (2014). https://doi.org/10.1016/j.ymssp.2013.11.010.
21. Y.F. Xu, D.M. Chen, and W.D. Zhu, Operational modal analysis using lifted continuously scanning laser Doppler vibrometer measurements and its application to baseline-free structural damage identification, *J. Vib. Control.* 25(7) 1341–1364 (2019). https://doi.org/10.1177/1077546318821154.
22. R.C. Gonzales, and R.E. Woods, (2018). *Digital image processing* (Pearson, New York, 2018).
23. G.D. Acar, and B.F. Feeny, Bend-bend-twist vibrations of a wind turbine blade. *Wind Energy,* 21(1) 15–28 (2018). https://doi.org/10.1002/we.2141.
24. Y. Chen, A.S.E. Mendoza, D.T. and Griffith, Experimental and numerical study of high-order complex curvature mode shape and mode coupling on a three-bladed wind turbine assembly. *Mech. Syst. Signal Process.* 160 107873 (2021). https://doi.org/10.1016/j.ymssp.2021.107873.
25. D.M. Chen, W.D. Zhu, Investigation of three-dimensional vibration measurement by three scanning laser Doppler vibrometers in a continuously and synchronously scanning mode. *J. Sound Vib.* 498 115950 (2021), https://doi.org/10.1016/j.jsv.2021.115950.
26. K. Yuan, and W.D. Zhu, Estimation of modal parameters of a beam under random excitation using a novel 3D continuously scanning laser Doppler vibrometer system and an extended demodulation method, *Mech. Syst. Signal Process.* 155 107606 (2021). https://doi.org/10.1016/j.ymssp.2021.107606.